Contributions to Mineralogy and Petrology (2018) 173:18
https://doi.org/10.1007/s00410-018-1445-6

ORIGINAL PAPER

The partitioning of sulfur between multicomponent aqueous fluids and felsic melts

Bernd Binder[1] · **Thomas Wenzel**[1] · **Hans Keppler**[2]

Received: 16 October 2017 / Accepted: 26 January 2018 / Published online: 2 February 2018

Abstract

Sulfur partitioning between melt and fluid phase largely controls the environmental impact of volcanic eruptions. Fluid/melt partitioning data also provide the physical basis for interpreting changes in volcanic gas compositions that are used in eruption forecasts. To better constrain some variables that control the behavior of sulfur in felsic systems, in particular the interaction between different volatiles, we studied the partitioning of sulfur between aqueous fluids and haplogranitic melts at 200 MPa and 750–850 °C as a function of oxygen fugacity (Ni–NiO or Re–ReO_2 buffer), melt composition (Al/(Na + K) ratio), and fluid composition (NaCl and CO_2 content). The data confirm a first-order influence of oxygen fugacity on the partitioning of sulfur. Under "reducing conditions" (Ni–NiO buffer), $D^{fluid/melt}$ is nearly one order of magnitude larger (323 ± 14 for a metaluminous melt) than under "oxidizing conditions" (Re–ReO_2 buffer; 74 ± 5 for a metaluminous melt). This effect is likely related to a major change in sulfur speciation in both melt and fluid. Raman spectra of the quenched fluids show the presence of H_2S and HS^- under reducing conditions and of SO_4^{2-} and HSO_4^- under oxidizing conditions, while SO_2 is undetectable. The latter observation suggests that already at the Re–ReO_2 buffer, sulfur in the fluid is almost completely in the S^{6+} state and, therefore, more oxidized than expected according to current models. CO_2 in the fluid (up to $x_{CO2} = 0.3$) has no effect on the fluid/melt partitioning of sulfur, neither under oxidizing nor under reducing conditions. However, the effect of NaCl depends on redox state. While at oxidizing conditions, $D^{fluid/melt}$ is independent of x_{NaCl}, the fluid/melt partition coefficient strongly decreases with NaCl content under reducing conditions, probably due to a change from H_2S to NaSH as dominant sulfur species in the fluid. A decrease of $D^{fluid/melt}$ with alkali content in the melt is observed over the entire compositional range under reducing conditions, while it is prominent only between the peraluminous and metaluminous composition in oxidizing experiments. Overall, the experimental results suggest that for typical oxidized, silicic to intermediate subduction zone magmas, the degassing of sulfur is not influenced by the presence of other volatiles, while under reducing conditions, strong interactions with chlorine are observed. If the sulfur oxidation state is preserved during an explosive eruption, a large fraction of the sulfur released from oxidized magmas may be in the S^{6+} state and may remain undetected by conventional methods that only measure SO_2. Accordingly, the sulfur yield and the possible climatic impact of some eruptions may be severely underestimated.

Keywords Sulfur · Haplogranite · Volcanic gases · Sulfur excess · Chlorine · Degassing

Communicated by Jochen Hoefs.

Electronic supplementary material The online version of this article (https://doi.org/10.1007/s00410-018-1445-6) contains supplementary material, which is available to authorized users.

✉ Hans Keppler
hans.keppler@uni-bayreuth.de

[1] Arbeitsbereich Mineralogie und Geodynamik, Universität Tübingen, Wilhelmstr. 56, 72074 Tübingen, Germany

[2] Bayerisches Geoinstitut, Universität Bayreuth, 95440 Bayreuth, Germany

Introduction

Sulfur compounds—mostly SO_2, but sometimes also H_2S and SO_3 or sulfate aerosols—occur in volcanic gases typically at the level of a few volume%, i.e. in quantities that are subordinate relative to H_2O and CO_2 (e.g. Devine et al. 1984; Symonds et al. 1994, Oppenheimer et al. 2011). Nevertheless, sulfur is mostly responsible for the short-term effect of explosive volcanic eruptions on climate, which is due to the cooling effect of sulfate aerosols in the stratosphere (e.g. McCormick et al. 1995; Robock 2002). Over long geologic

periods, the balance between CO_2 emissions by volcanoes and CO_2 sequestration by weathering, sedimentation, and subduction controls climate (e.g. McKenzie et al. 2016), but the CO_2 emissions even of very large individual eruptions are typically unable to alter this balance. On the other hand, severe cooling may well result from one single eruption and there is generally a good correlation between the surface temperature record over the last centuries and estimates of sulfur loading (Briffa et al. 1998; Sigl et al. 2015). Aside from sulfur compounds and CO_2, volcanic HCl may also have an environmental impact by reducing ozone concentrations in the stratosphere, but this effect is more controversial (Black et al. 2014; Gutiérrez et al. 2016).

The mineralization in magmatic-hydrothermal ore deposits is another process that is strongly affected by the behavior of sulfur and chlorine. Under reducing conditions, the precipitation of sulfides may prevent the enrichment of elements such as Cu or Ag to economic grades during fractional crystallization. However, upon water saturation, sulfur species may be potent ligands that enhance the partitioning of trace metals into ore-forming fluids (e.g. Zajacz and Halter 2009). Accordingly, considerable efforts have been made to understand sulfur partitioning between silicate melts and fluids. It is now probably generally accepted that oxygen fugacity is the prime variable controlling sulfur partitioning. If oxygen fugacity changes from oxidizing conditions (e.g. the Re–ReO_2 or Fe_2O_3–Fe_3O_4 buffer) to more reducing conditions, a drastic increase of the fluid/melt partition coefficient of sulfur $D_S^{fluid/melt}$ by about one order of magnitude occurs near the Ni–NiO buffer. This effect, which was first observed by Keppler (1999) in a haplogranitic model system, has now also been confirmed for other melt compositions (Webster and Botcharnikov 2011; Zajacz et al. 2012). The effect is likely related to profound changes in sulfur speciation both in the silicate melt and in the coexisting fluid. In the silicate melt, S^{6+} dominates under oxidizing conditions but is reduced to S^{2-} at lower oxygen fugacity (e.g. Carroll and Rutherford 1988; Jugo et al. 2010; Wilke et al. 2011). In magmatic-hydrothermal fluids, SO_3 and its hydrated forms (e.g. H_2SO_4) are first reduced to SO_2 and then to H_2S (Binder and Keppler 2011; Ni and Keppler 2012). After oxygen fugacity, the bulk composition of the silicate melt may be the next most important parameter influencing sulfur partitioning (e.g. Webster and Botcharnikov 2011; Fiege et al. 2014, 2015; Zajacz 2015; Beermann et al. 2015; Masotta et al. 2016); in general, $D_S^{fluid/melt}$ increases from depolymerized basic melts to highly polymerized silicic magmas and numerical models for predicting the effect of melt composition have been developed (Masotta et al. 2016). Compared to oxygen fugacity and melt composition, the effect of pressure and temperature on the behavior of sulfur appears to be subordinate (Keppler 2010). However, the fluids released from degassing magmas usually contain several components in addition to H_2O and sulfur species, most notably CO_2 and chloride. With the notable exception of the study by Webster et al. (2011), the interaction of these different fluid species with sulfur has not yet been systematically investigated, although some experiments involving multicomponent fluids are described in the literature (Webster et al. 2009; Lesne et al. 2011; Fiege et al. 2014, 2015). The main purpose of this study is, therefore, to quantify the effect of CO_2 and of chloride (in the form of NaCl) on the behavior of sulfur in felsic systems. In addition, the effect of strongly peralkaline or peraluminous compositions on the behavior of sulfur has also been investigated. These studies were carried out with a haplogranitic base composition, because such a compositionally simple system allows the physical parameters affecting sulfur partitioning to be readily identified.

Methods

Starting materials

Starting materials for all experiments were haplogranitic glasses and dilute solutions of sulfuric acid H_2SO_4. Sulfuric acid solutions were prepared by diluting a certified standard solution. In some experiments, oxalic acid or NaCl were added to produce CO_2-bearing or saline fluids. Haplogranitic glasses were synthesized from stoichiometric mixtures of analytical grade SiO_2 (99.99%), $Al(OH)_3$ (99.9%), Na_2CO_3 (99.9%), and $KHCO_3$ (99.5%). The mixtures were ground up in a ceramic ball mill under ethanol for 30 min. The dried mixtures were then decarbonated in a platinum crucible by slowly heating to 1100 °C during 12 h, followed by 1–2 h at a constant temperature of 1100 °C. The crucible was then quenched in distilled water, the glass ground to a powder and then melted again in a Pt crucible at 1600 °C for 1–2 h. After quenching in water, the glass was again ground up to a fine powder. X-ray fluorescence-analyses of the glasses produced are given in Table 1. One glass is distinctly peraluminous in composition, one is peralkaline and one was intended to have a molar Al/(Na + K) ratio of 1, while the measured ratio is slightly below 1. Due to the preferential dissolution of alkalies in the fluid, the latter composition often approached a molar Al/(Na + K) ratio of 1 in the subsequent partitioning experiments.

High-pressure experiments

All experiments were carried out at 200 MPa and 750–850 °C with rapid-quench cold-seal vessels made of the Ni-based super alloy IN 713 LC, using water as pressure medium. The sample capsule was mounted on the end of a filler rod, which was held in the hot zone of the vessel by an external magnet during a run. To terminate an experiment,

Table 1 Composition of glasses used as starting materials

	SiO_2 (wt%)	Al_2O_3 (wt%)	Na_2O (wt%)	K_2O (wt%)	Al/(Na + K) (molar)
Haplogranite	76.98 (5)	12.11 (6)	4.80 (3)	4.78 (1)	0.93
Peraluminous haplogranite	76.45 (5)	14.31 (6)	4.71 (3)	4.05 (1)	1.18
Peralkaline haplogranite	80.20 (5)	9.98 (6)	4.91 (3)	4.22 (1)	0.79

Compositions were determined by X-ray fluorescence on powder pellets, to avoid alkali losses. Values in brackets are one standard deviation in the last digit

the sample was dropped into a water-cooled zone and quenched to room temperature within a few seconds. Temperature was measured by a type K thermocouple in an external drill hole close to the sample capsule. Temperatures reported are accurate to ± 5 °C. Pressure was measured with a Hesch Type HE 012.1 gauge, which was calibrated against a Heise CM bourdon-type gauge with a specified precision of 0.1%. Measured pressures are accurate to ± 2 MPa. The run duration for all experiments was 7 days. Calculations using the permeability data of Chou (1986) showed that this run duration would allow more than enough hydrogen to diffuse from an external Ni–NiO buffer into the capsule to reduce all the H_2SO_4 to H_2S. Indeed, Raman spectrometric analyses of fluid inclusions (see below) confirmed that the charges had fully equilibrated with the external buffer. Moreover, the absence of any detectable compositional gradients in microprobe analyses of quenched glasses suggests that chemical equilibrium between melt and fluid was reached. In a previous study on sulfur partitioning in the haplogranite-fluid system (Keppler 2010), run durations were varied between 1 and 64 days, with the result that already after 8 days, the partition coefficients were within analytical error of those obtained after 64 days.

Sample capsules were made of gold (25 mm long, 2.5 mm outer diameter, wall thickness 0.2 mm), which does not dissolve any sulfur under run conditions (Keppler 1999). Capsules were usually filled with about 20 mg of glass powder and 20 mg of dilute H_2SO_4 solution (+ NaCl or oxalic acid in some experiments) and sealed by arc welding. They were checked for leaks by weighing before and after heating to 150 °C for 10 h. Only capsules without weight loss upon heating were used. Oxygen fugacity was controlled by external buffers. For the Re–ReO_2 buffer ("oxidizing conditions"), a standard double capsule technique was used. The sample capsule was sealed into an outer gold capsule (35 mm long, outer diameter 5 mm, wall thickness 0.2 mm) together with a mixture of Re and ReO_2 (weight ratio 1:9) and some water. For the Ni–NiO buffer ("reducing conditions"), a double capsule technique was not feasible, since Ni rapidly diffuses through the gold into the inner capsule and reacts with the sulfur. Instead, an open gold capsule (35 mm long, 5 mm outer diameter, 0.2 mm wall thickness) filled with a 1:1 mixture of Ni and NiO was placed directly below the sample capsule in the autoclaves; together with the water used as pressure medium, this provided efficient buffering of oxygen fugacity.

Investigation of run products

After quenching, sample capsules were checked for leaks by weighing; capsules with significant weight loss were discarded. The buffers were controlled by X-ray diffraction to assure that both buffering phases were still present after the experiment. Quenched glasses were embedded in Crystalbond 509 resin, polished and carbon-coated for microprobe analysis. Chemical compositions were determined using a JEOL JXA-8900R electron microprobe with 20 kV acceleration voltage and 20 nA beam current. 30 to 40 points were analyzed for each sample and the results were averaged. To reduce beam damage, a 20-µm defocused beam was used. Na was always measured first with an accumulation time of 8 s to minimize evaporation losses. The other major elements were measured for 16–30 s. Due to its low concentration, the counting time for sulfur was 120 s. Sulfur was always measured twice with a program using a $BaSO_4$ standard and a separate program using CuS as a standard, to account for possible effects of oxidation state on peak positions and X-ray yields. However, the results of the two programs were always identical within error. Raman spectra of fluid inclusions in the quenched glasses were measured with a confocal Labram 2 (Dilor/Horiba Jobin Yvon) spectrometer with a 1800-mm^{-1} grating and a Peltier-cooled CCD detector using the 488 nm line of an argon laser for excitation. The accumulation time for individual spectra was 30 s, with a laser power of 11 mW at the sample. Sulfur concentrations in the fluid were calculated by mass balance. This is justified by the observation that the sulfur content of the gold on the inner surface of the sample capsule was always below the detection limit of the electron microprobe (< 60 ppm), such that any sulfur loss to the capsule can be neglected.

Results and discussion

System halogranite–S–H_2O–CO_2

Supplementary Table 1 (online resource) compiles the experimental results on the fluid/melt partitioning of sulfur

in the system haplogranite–S–H_2O–CO_2. Run products of experiments at the Ni–NiO buffer were glasses with an olive-green color, probably due to some reduced sulfur (polysulfide) species, while under oxidizing conditions (Re–ReO_2 buffer) the glasses were colorless. Abundant fluid inclusions were always observed. The molar fractions of CO_2 quoted refer to the fluid composition at the beginning of the experiment. The preferential dissolution of H_2O in the melt increases x_{CO2} during the run. However, due to the high fluid/melt ratio (near 1:1 by weight), this effect is very minor. Mass balance calculations show that the dissolution of 6–8 wt% H_2O in the melt increases x_{CO2} by 0.01 to 0.02 (e.g. from 0.10 to 0.11).

Figure 1 shows the partitioning of sulfur between fluid and melt under reducing conditions. All data follow one single trend that can be described by a fluid/melt partition coefficient $D_S^{fluid/melt} = 323 \pm 14$. No obvious effect of temperature (750 or 850 °C) or of CO_2 content is detectable. However, due to the generally very small sulfur contents in the quenched melt, the analytical uncertainties in the data are relatively large. Note that here and in the following diagrams, we always assume that the trend line describing the partitioning of sulfur between the two coexisting phases passes through the origin. This is required by the fact that in equilibrium, the chemical potentials of sulfur in the two phases have to be the same.

The microprobe analyses of the quenched glasses (Supplementary Table 1) show low totals due to the elevated water contents. If the analyses are renormalized to 100% and compared with the starting material (Table 1), the main difference is that about 0.3 wt% Na_2O were apparently leached out of the melt into the fluid. However, this effect is so small that the Al/(Na + K) ratio remained nearly unchanged; the average value for the experiments under reducing conditions in Supplementary Table 1 is 0.92 ± 0.02. Raman spectra of the liquid and gas phase of fluid inclusions from these experiments (Fig. 2) show H_2S as the only sulfur species (band at 2590 cm^{-1}), together with the bands of water and of CO_2 for the CO_2-bearing runs.

Compared to the results for reducing conditions, the experiments at the Re–ReO_2 buffer yielded much higher sulfur concentrations in the melt phase and a reduction of the fluid/melt partition coefficient to $D_S^{fluid/melt} = 74 \pm 5$ (Fig. 3). Again, no systematic effect of CO_2 on the behavior of sulfur is detectable. However, there is significant scatter of the data points around the regression line. A possible reason is that the partitioning of sulfur is extremely sensitive to oxygen fugacity and the deviations from the regression curve may be related to subtle variations in f_{O2} between the experiments. This is plausible, since in these experiments, oxalic acid was added as a source of CO_2, which requires oxidation by equilibration with the external buffer. If the microprobe analyses of the quenched glasses (Supplementary Table 1) are renormalized to 100% and compared with the starting composition (Table 1), the main difference appears to be a loss of about 0.5 wt% Na_2O to the fluid, which caused the Al/(Na + K) ratio to increase from 0.93 to 0.96 ± 0.02. Raman spectra of the fluid inclusions in run product glasses showed that all sulfur was present as S^{6+}; bands of SO_4^{2+} and of HSO_4^- are prominent in the Raman spectra of the liquid phases in both CO_2-free and CO_2-bearing runs, while no sulfur species were detectable in the gas phase (Fig. 4). The presence of HSO_4^- implies a rather acidic pH of the quenched fluid.

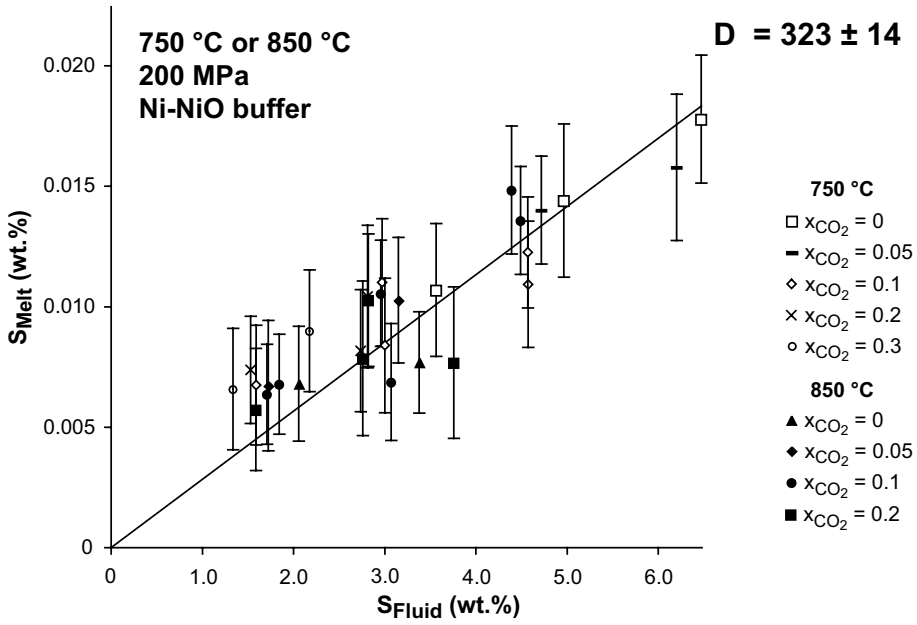

Fig. 1 Partitioning of sulfur between fluid and melt in the system haplogranite–S–H_2O–CO_2 at Ni–NiO buffer conditions. Error bars denote one standard deviation

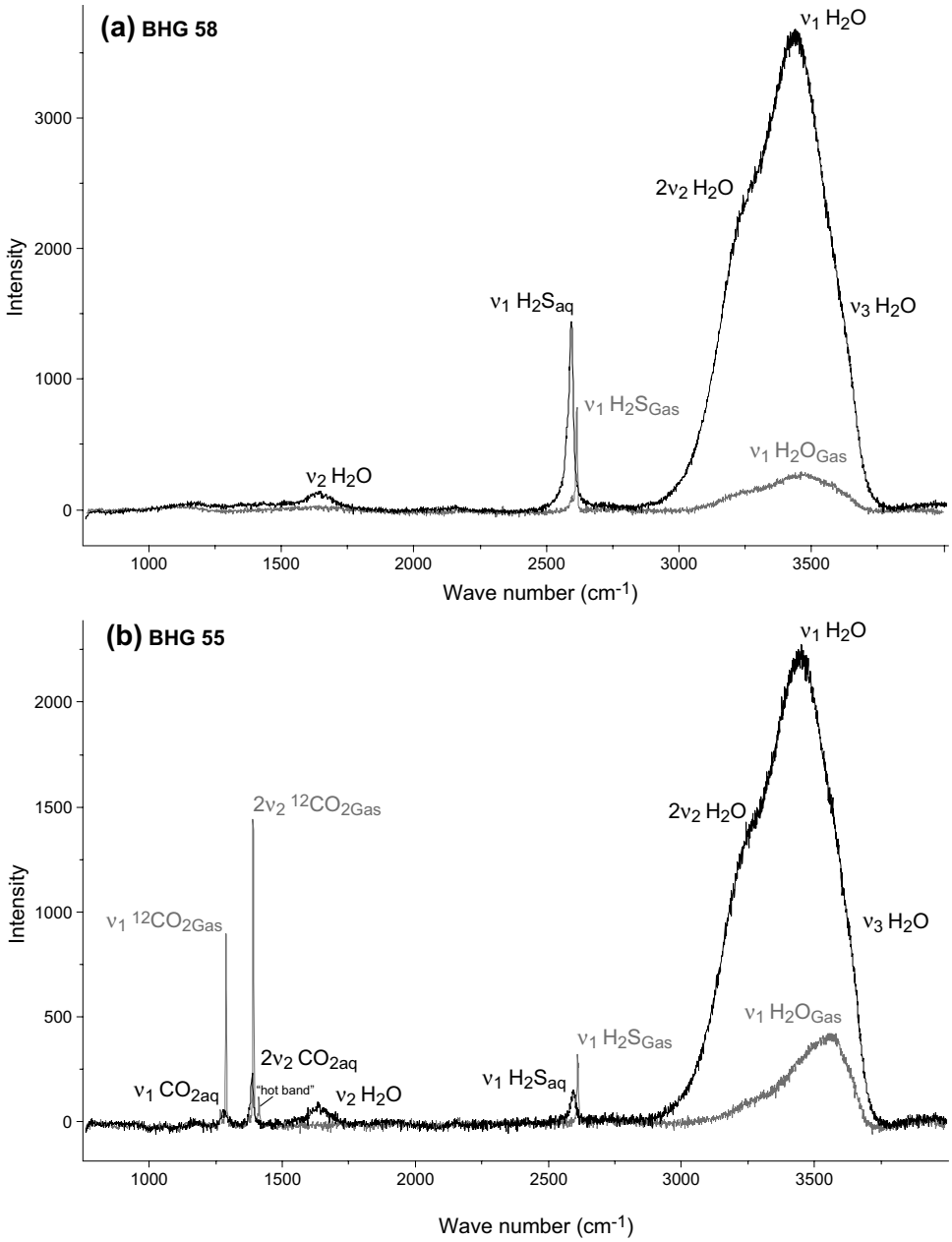

Fig. 2 Raman spectra of fluid inclusions from experiments in the system haplogranite–S–H_2O–CO_2 at Ni–NiO buffer conditions. Gray = gas phase; black = liquid phase. **a** Experiment BHG 58, $x_{CO2} = 0$; **b** experiment BHG 55, $x_{CO2} = 0.2$

The absence of an effect of CO_2 on the fluid/melt partitioning of sulfur observed here is entirely consistent with the results of Webster et al. (2011), while the absence of a notable temperature effect is consistent with Keppler (1999, 2010). The fluid/melt partition coefficient $D_S^{fluid/melt} = 323 \pm 14$ observed under Ni–NiO buffer conditions is below the value of 468 ± 32 at the Co–CoO buffer under otherwise equal conditions (Keppler 1999, 2010), which likely reflects the effect of oxygen fugacity on sulfur partitioning. The value for $D_S^{fluid/melt} = 74 \pm 5$ at Re–ReO_2 buffer conditions is somewhat higher than that reported for the hematite–magnetite buffer (49 ± 2, Keppler 2010), which may again reflect the effect of different oxygen fugacity or perhaps also slight differences in the Al/(Na + K) ratio of the starting materials.

The observation that CO_2 does not affect the partitioning of sulfur may be related to the very low solubility of CO_2 in the silicate melt under run conditions (Webster et al. 2011), which makes any interaction between sulfur and CO_2 in the melt unlikely. Moreover, at 200 MPa and 750–850 °C, there are only mild deviations from ideality expected in the H_2O–CO_2 gas phase (Kerrick and Jacobs 1981). For reducing conditions, where H_2S appears to be the dominant species in the fluid, one may therefore assume that the mixing of H_2O, CO_2, and H_2S in the gas phase is also close to ideality, which may explain why diluting H_2O by CO_2 does not affect

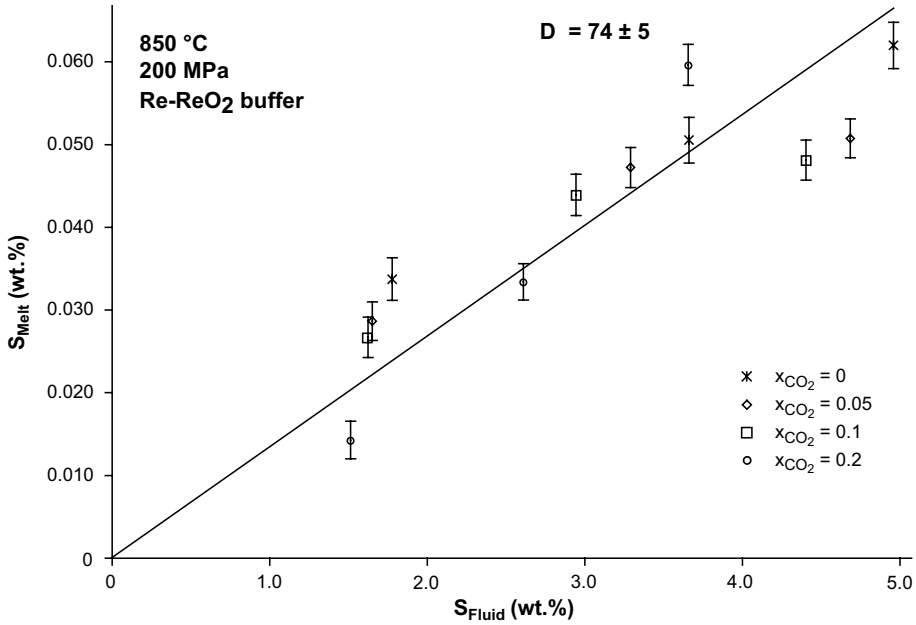

Fig. 3 Partitioning of sulfur between fluid and melt in the system haplogranite–S–H_2O–CO_2 at Re–ReO_2 buffer conditions. Error bars denote one standard deviation

the partitioning of sulfur. However, the absence of a CO_2 effect on sulfur partitioning under oxidizing conditions is more difficult to understand. One would expect species of S^{6+} to be strongly hydrated in the fluid and, therefore, changing water activity should affect the behavior of sulfur. A possible explanation for the absence of such an effect could be that the degree of hydration of the S^{6+} in fluid and melt is similar and they are similarly affected by reducing water activity in the system.

System halogranite–S–H_2O–NaCl

Experimental data on the fluid/melt partitioning of sulfur in the system halogranite–S–H_2O–NaCl are compiled in Supplementary Table 2 (online resource). Run product glasses contained abundant three-phase fluid inclusions with NaCl crystals, a gas phase and a liquid water-rich phase. Figure 5 demonstrates that unlike CO_2, NaCl has a strong effect on sulfur partitioning under reducing (Ni–NiO buffer) conditions. With increasing molar fraction of NaCl in the fluid $D_S^{fluid/melt}$ decreases from 323 ± 14 to 84 ± 12 at $x_{NaCl} = 0.3$. Inspection of the microprobe data in Supplementary Table 2 shows that compared to the starting material (Table 1), Na_2O contents in the melt increased, while K_2O contents decreased due to ion exchange with the fluid. The overall Al/(Na + K) ratio also increased from 0.93 to a maximum of 0.98 in all samples. If the microprobe analyses of the hydrous run product glasses are renormalized to 100% and compared to the starting material, it appears that on average the samples have gained about 1.8 wt% Na_2O, while they lost almost 3 wt% K_2O. Raman spectra (Fig. 6) of the fluid inclusions show H_2S as only sulfur species in the gas phase. However, in the liquid phase, a band is present near 2570 cm^{-1}, which is suggestive of HS^- rather than H_2S (Peltzer et al. 2016). This observation may indicate a more alkaline quench pH of the fluid. It may further imply that upon increasing NaCl content, the dominant sulfur species in the fluid changes from H_2S to NaSH. As H_2S is expected to be more volatile than NaSH, this would provide an obvious explanation for the reduction of $D_S^{fluid/melt}$ with increasing NaCl in the fluid.

Under oxidizing conditions (Re–ReO_2 buffer), the presence of NaCl does not appear to affect the behavior of sulfur (Fig. 7). The measured partition coefficient $D_S^{fluid/melt} = 128 \pm 6$ is independent of NaCl concentration (ranging from $x_{NaCl} = 0.1$ to 0.3). The difference of this value to that measured in the NaCl-free haplogranite system under otherwise equal conditions (74 ± 5) is likely related to a change in melt composition caused by the exchange with the fluid, since the Al/(Na + K) ratio increased significantly from the initial value of 0.93 to an average of 1.08 ± 0.03. This change apparently occurred mainly between the NaCl-free composition and that with $x_{NaCl} = 0.1$. Between $x_{NaCl} = 0.1$ and 0.3, there is little further change in melt composition, which explains why $D_S^{fluid/melt}$ remains constant. If the analyses of the hydrous glasses are renormalized to 100% and compared with the starting material, the Na_2O content increased on average by about 1 wt%, while the K_2O content decreased by about 3.1 wt%. Overall, these data suggest a stronger partitioning of alkalis into the fluid than under reducing conditions, with the effect that the melts become peraluminous. This compositional difference is particularly obvious, when the data are compared with the NaCl-free haplogranite system, while increasing the NaCl concentration in the fluid from $x_{NaCl} = 0.1$ to 0.3 has only a subordinate

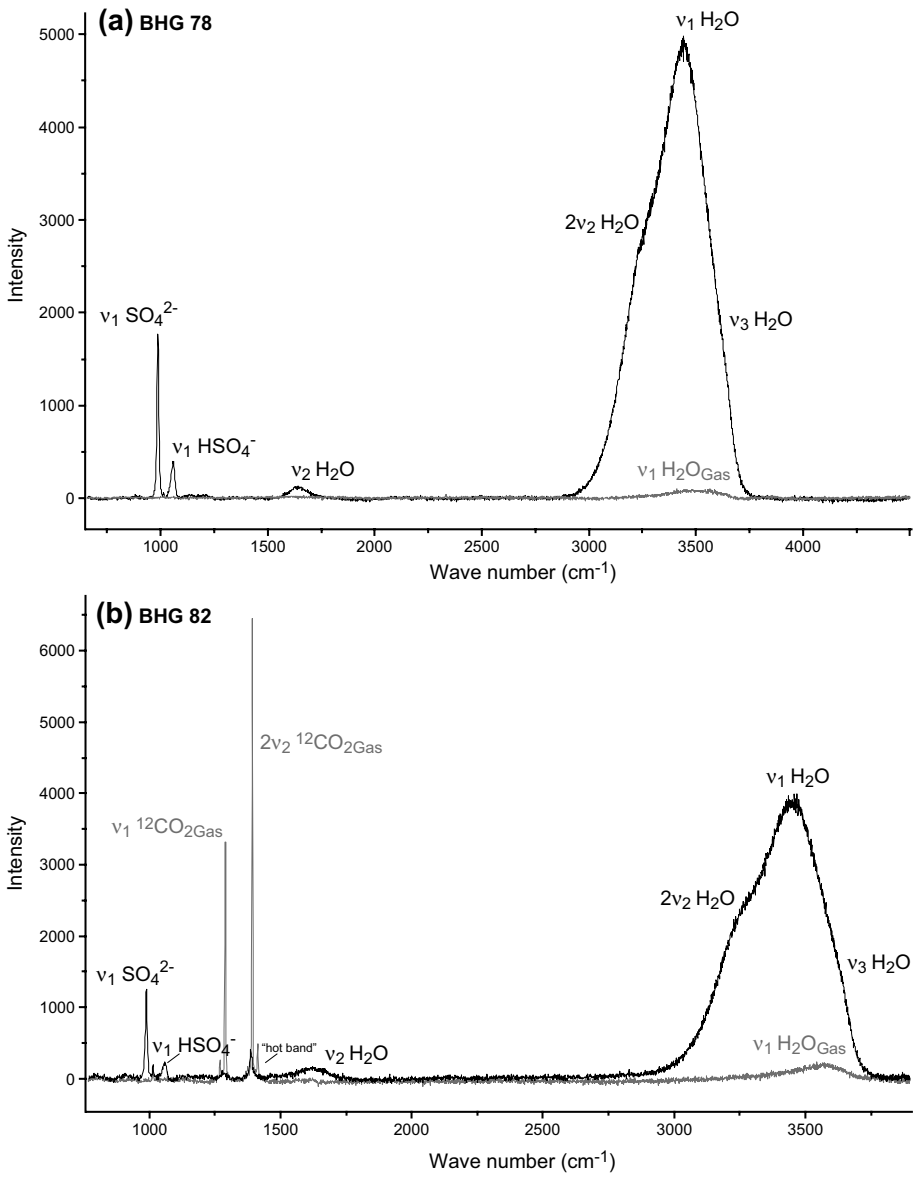

Fig. 4 Raman spectra of fluid inclusions from experiments in the system haplogranite–S–H_2O–CO_2 at Re–ReO_2 buffer conditions. Gray = gas phase; black = liquid phase. **a** Experiment BHG 78, $x_{CO2} = 0$; **b** experiment BHG 82, $x_{CO2} = 0.2$

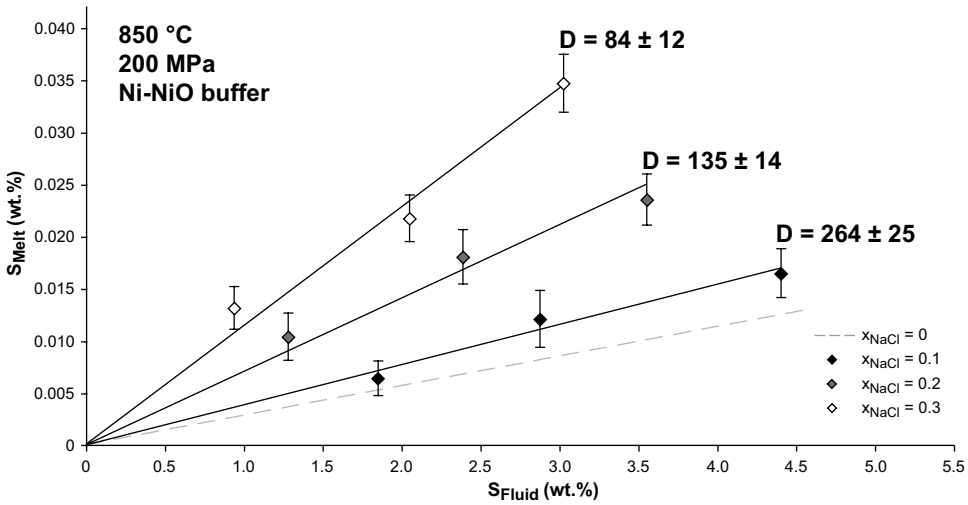

Fig. 5 Partitioning of sulfur between fluid and melt in the system haplogranite–S–H_2O–NaCl at Ni–NiO buffer conditions. The dotted line is from Fig. 1 and corresponds to a $D_S^{fluid/melt} = 323 \pm 14$. Error bars denote one standard deviation

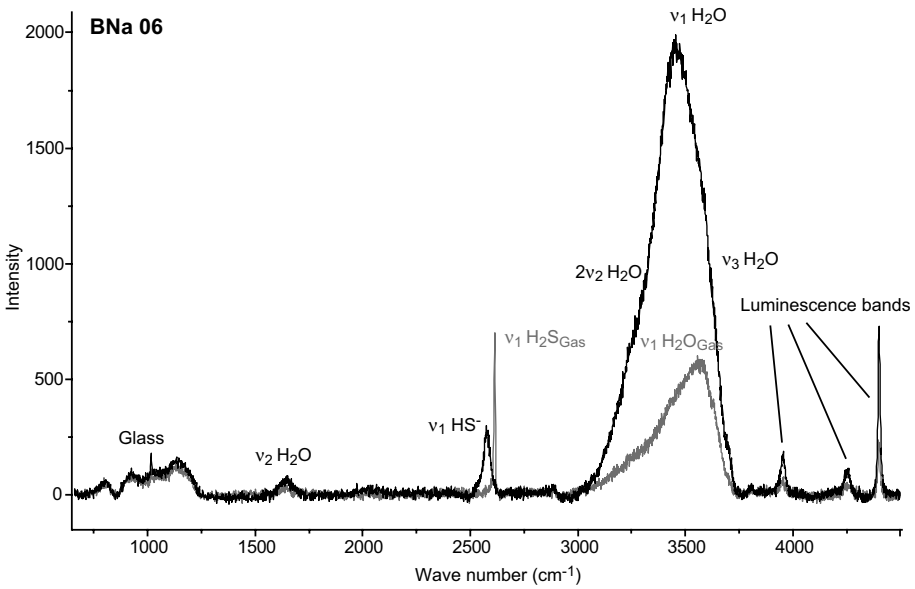

Fig. 6 Raman spectra of a fluid inclusion from experiment BNa06 in the system haplogranite–S–H_2O–NaCl at Ni–NiO buffer conditions. Gray = gas phase; black = liquid phase. The sharp bands at high frequency (near 4000 cm^{-1}) are due to luminescence of some unknown species; this was confirmed by changing the excitation wavelength of the laser, which caused these bands to shift in the Raman spectrum

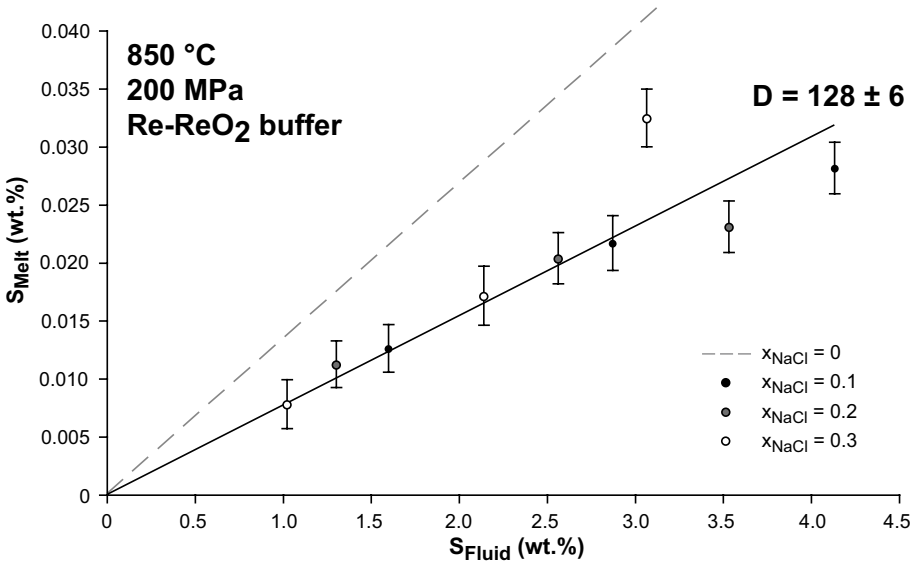

Fig. 7 Partitioning of sulfur between fluid and melt in the system haplogranite–S–H_2O–NaCl at Re–ReO_2 buffer conditions. Error bars denote one standard deviation

effect on melt composition and, therefore, $D_S^{fluid/melt}$ is not further affected. Raman spectra of fluid inclusions (Fig. 8) from NaCl-bearing experiments run under oxidizing conditions show only species of S^{6+} in the form of SO_4^{2-} and HSO_4^- in the liquid phase. As for CO_2, the absence of an effect of NaCl on the sulfur partitioning is somewhat unexpected, since NaCl affects water activity and, therefore, the hydration state of S^{6+} in the fluid.

The data in Supplementary Table 2 include the Cl contents of the quenched glasses and, therefore, also allow the effect of sulfur in the fluid on the partitioning of Cl to be quantified. In the reducing experiments at the Ni–NiO buffer, no effect of sulfur on the behavior of Cl can be detected. However, the runs with the Re–ReO_2 buffer show a clear decrease of $D_{Cl}^{fluid/melt}$ with increasing sulfur concentration (Fig. 9). For example, for $x_{NaCl} = 0.3$, $D_{Cl}^{fluid/melt}$ decreases from 98 at 1 wt% sulfur in the fluid to 75 at 3.1 wt% S.

The effect of peralkaline and peraluminous melt compositions

Supplementary Table 3 (online resource) compiles the experimental data on the fluid/melt partitioning of sulfur in the system haplogranite–S–H_2O for peralkaline and peraluminous melt compositions. At the Ni–NiO buffer, $D_S^{fluid/melt}$ continuously increases with the Al/(Na + K) ratio, from 257 ± 17 for peralkaline melts to 508 ± 15 for

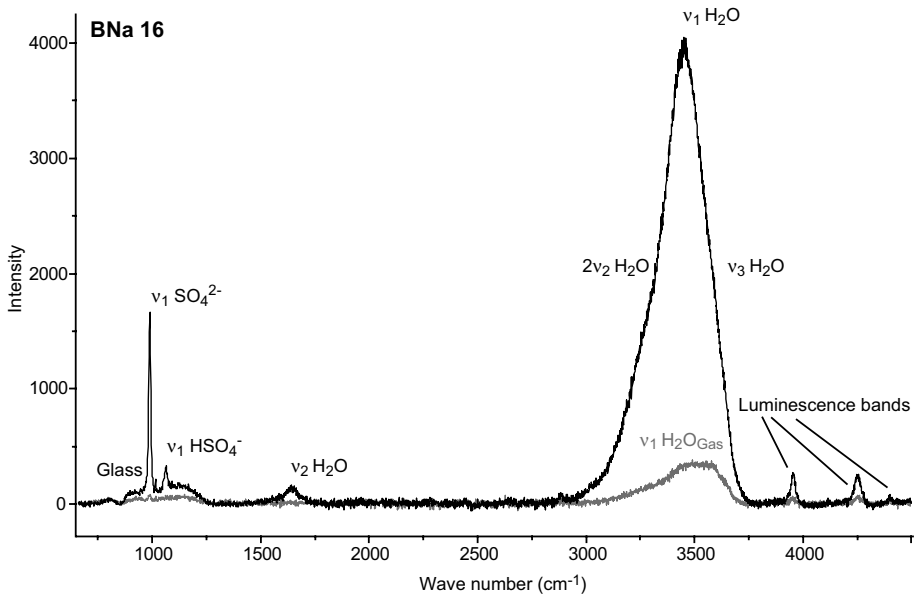

Fig. 8 Raman spectra of a fluid inclusion from experiment BNa16 in the system haplogranite–S–H_2O–NaCl at Re–ReO_2 buffer conditions. Gray = gas phase; black = liquid phase. The sharp bands at high frequency (near 4000 cm^{-1}) are due to luminescence of some unknown species

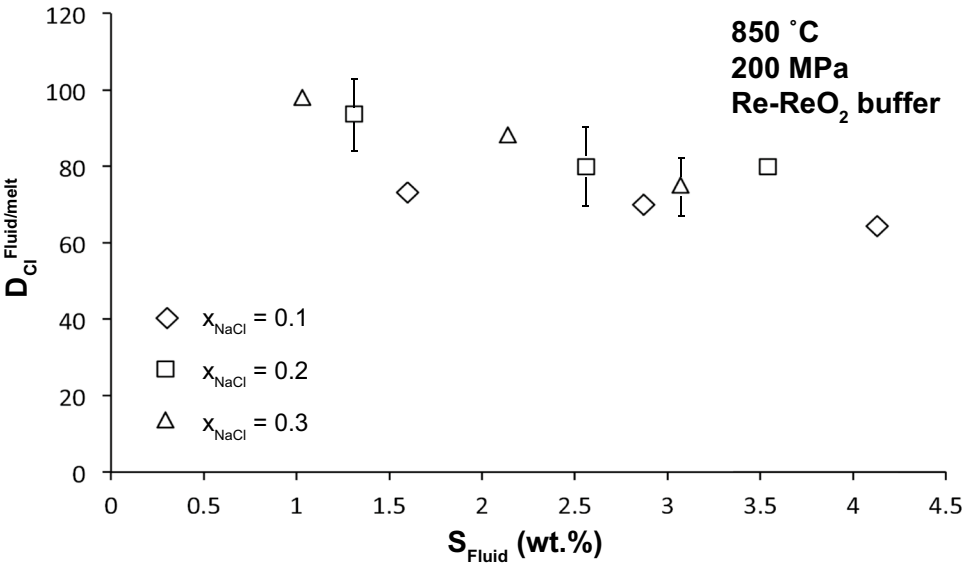

Fig. 9 Partitioning of chlorine between fluid and melt in the system haplogranite–S–H_2O–NaCl at Re–ReO_2 buffer conditions

peraluminous melts (Fig. 10). Microprobe analyses of run products (Supplementary Table 3) suggest that for all compositions, about 0.2 to 0.3 wt% Na_2O were leached out into the fluid. This effect becomes obvious after renormalizing the chemical analyses of the hydrous glasses to 100% and comparing them with the starting compositions in Table 1. Raman spectra of fluid inclusions in the run product glasses (Fig. 11) show H_2S as the only sulfur species in the gas phase for all compositions. However, in the quenched liquid, HS^- coexists with H_2S for the peralkaline compositions, while only H_2S is detected for the peraluminous melts. As in the NaCl-bearing experiments, this may imply a change of the fluid speciation of sulfur, from H_2S in the peraluminous system to NaSH in the peralkaline system, which may explain the variation in $D_S^{fluid/melt}$.

At the Re–ReO_2 buffer, $D_S^{fluid/melt}$ increased to 246 ± 9 for a peraluminous composition with Al/(Na + K) = 1.18, while the peralkaline starting material yielded a partition coefficient of 96 ± 12 (Fig. 12). The leaching of Na_2O into the fluid is generally stronger than under reducing conditions. After renormalization of the data to 100% for a dry glass, the numbers in Supplementary Table 3 suggest that from the peralkaline glasses on average 1.2 wt% of Na_2O were leached into the fluid, but only 0.3–0.4 wt% from the peraluminous glasses. The high Na_2O loss from the peralkaline glass had the effect that Al/(Na + K) increased to 0.95–1, comparable to the experiments with the normal

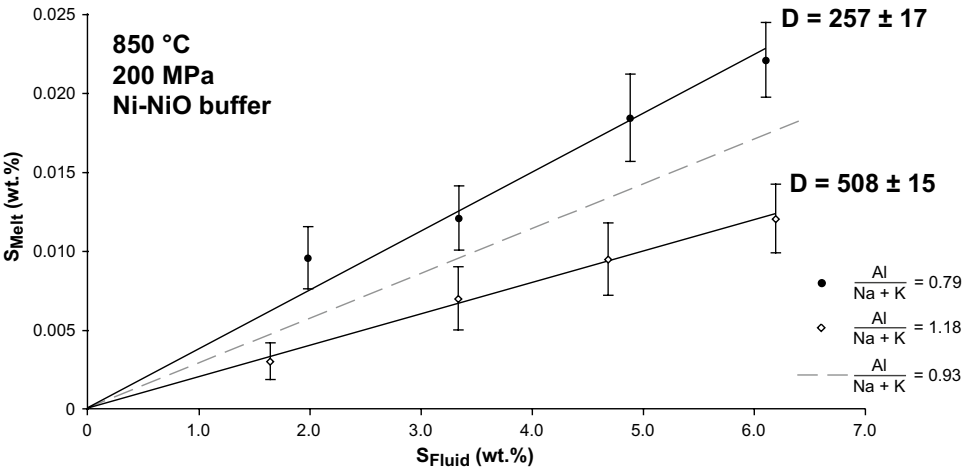

Fig. 10 Partitioning of sulfur between fluid and peralkaline or peraluminous melts in the system haplogranite–S–H_2O at Ni–NiO buffer conditions. The dotted line is from Fig. 1 and corresponds to a $D_S^{fluid/melt} = 323 \pm 14$. Error bars denote one standard deviation

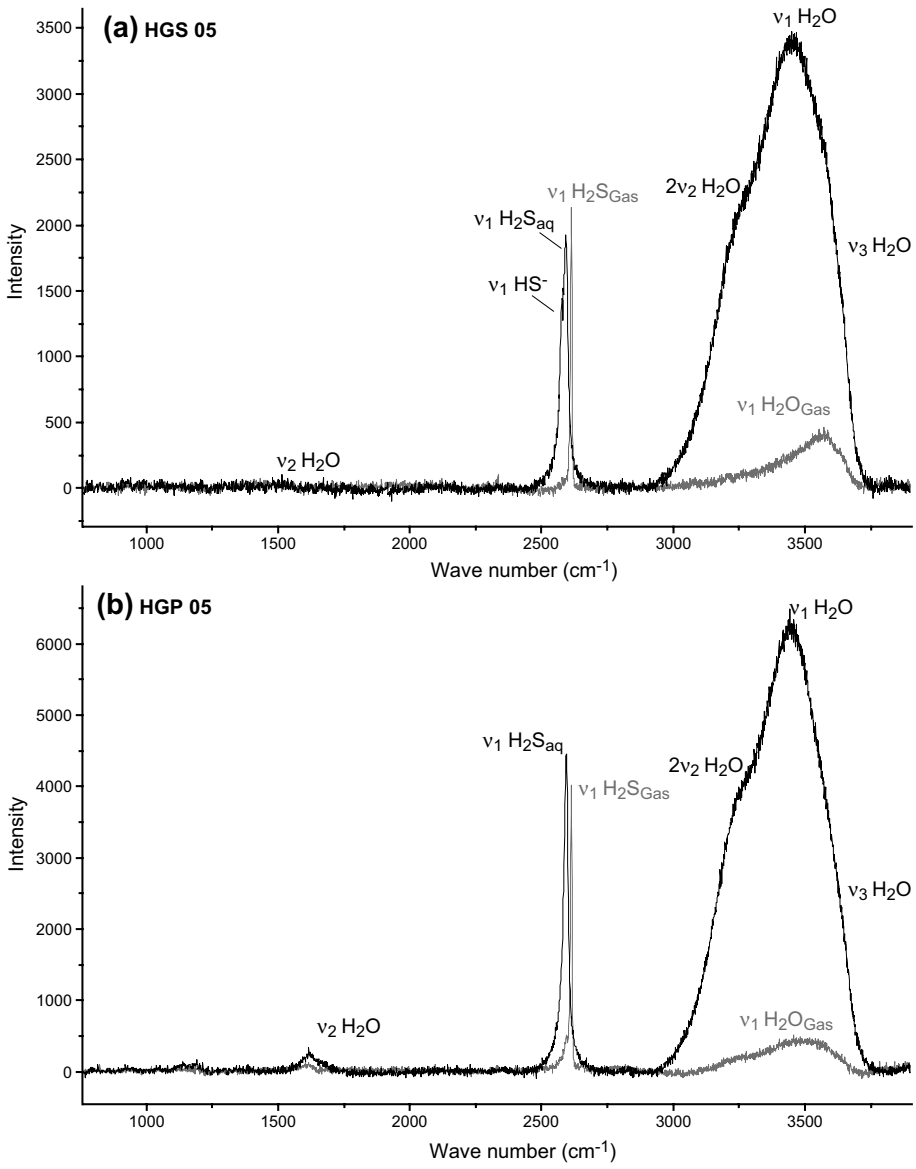

Fig. 11 Raman spectra of fluid inclusions from experiments in the system haplogranite–S–H_2O at Ni–NiO buffer conditions. Gray = gas phase; black = liquid phase. **a** Experiment HGS 05 with a peralkaline melt; **b** experiment HGP 05 with a peraluminous melt

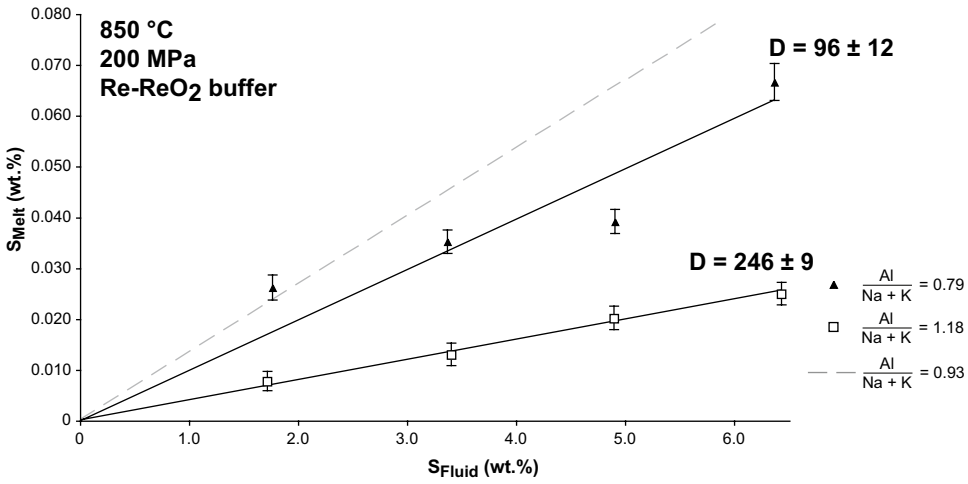

Fig. 12 Partitioning of sulfur between fluid and peralkaline or peraluminous melts in the system haplogranite–S–H_2O at Re–ReO_2 buffer conditions. The dotted line is from Fig. 3 and corresponds to a $D_S^{fluid/melt} = 74 \pm 5$. Error bars denote one standard deviation

haplogranitic composition in Supplementary Table 1 and Fig. 3. Sulfur was only detected in the liquid phase of the fluid inclusions in run product glasses; however, the ratio of SO_4^{2-} to HSO_4^- is distinctly higher for the peralkaline glasses than for the peraluminous ones (Fig. 13), indicating less acidic quench fluids in the peralkaline system. Again, this may imply a change of the dominant fluid species of sulfur from Na_2SO_4 in the peralkaline system to $NaHSO_4$ or H_2SO_4 in the peraluminous system, which may be the main reason for the observed variation in the sulfur partition coefficient. However, melt composition probably also plays some role. Indeed, experiments on anhydrite ($CaSO_4$) solubility in silicate melts show a strong increase of equilibrium sulfate concentration in the melt with depolymerization (Masotta and Keppler 2015).

Implications for sulfur degasing

A main objective of this study was to investigate possible interactions between CO_2, NaCl, and sulfur during magmatic degassing. The experiments were carried out in a simple Ca and Fe-free model system to facilitate the interpretation of the data. The presence of Fe in the system, for example, could have caused redox reactions with sulfur to occur during quenching, such that the oxidation state of sulfur during the run could not have been quantified by Raman spectroscopy of quenched fluid inclusions. CaO may cause the precipitation of anhydrite under oxidizing conditions (Masotta and Keppler 2015), which would have made it difficult to accurately determine fluid compositions by mass balance. However, despite the simplifications in the model system studied, we suggest that the basic observations made are likely applicable to a range of natural magmas of intermediate to acidic composition. In these magmas, FeO is typically only a minor component, while CaO may occur in moderate concentrations. However, neither FeO nor CaO are expected to strongly partition into the fluid phase, where possible interactions between CO_2, NaCl, and sulfur species may occur. In the melt phase, the concentrations of C, Cl, and S are so small that interactions are unlikely. Moreover, the data analysis of Masotta et al. (2016) suggests that at least under oxidizing conditions, melt composition affects $D_S^{fluid/melt}$ primarily through the overall structure of the melt, as indicated by the ASI and nbo/t parameters; FeO has no statistically significant additional effect, while a minor effect of the $CaO/(Na_2O + K_2O)$ ratio is observed.

Table 2 summarizes the experimental observations made in this study. The data suggest that for oxidized, silicic to intermediate magmas, sulfur degassing is likely independent of the presence of other volatiles (CO_2 and chlorine), while under reducing conditions, strong interactions with NaCl occur. Since large explosive eruptions that may have a significant effect on global surface temperatures typically occur above subduction zones, where magmas tend to be relatively oxidized, this means that interactions between volatiles during degasing can be mostly ignored in forecasting stratospheric sulfur loading. The numerical model by Masotta et al. (2016) predicts the fluid/melt partition coefficients measured at the Re–ReO_2 buffer within a factor of two or better (see Fig. 10 b of Masotta et al. 2016); given that this model covers a wide compositional range with partition coefficients varying over more than two orders of magnitude, this result is quite satisfactory. However, certain details, such as the strong increase of $D_S^{fluid/melt}$ for peraluminous melts are not properly predicted. Moreover, while the Masotta et al. (2016) model parameterizes $D_S^{fluid/melt}$ exclusively as a function of melt composition, the Raman spectroscopic data of the present study clearly show that major changes in fluid speciation—which occur in response to changing melt composition—may actually be driving the variation in fluid/melt partition coefficients.

The sulfur speciation as recorded by the Raman spectra of quenched fluids in fluid inclusions may have important

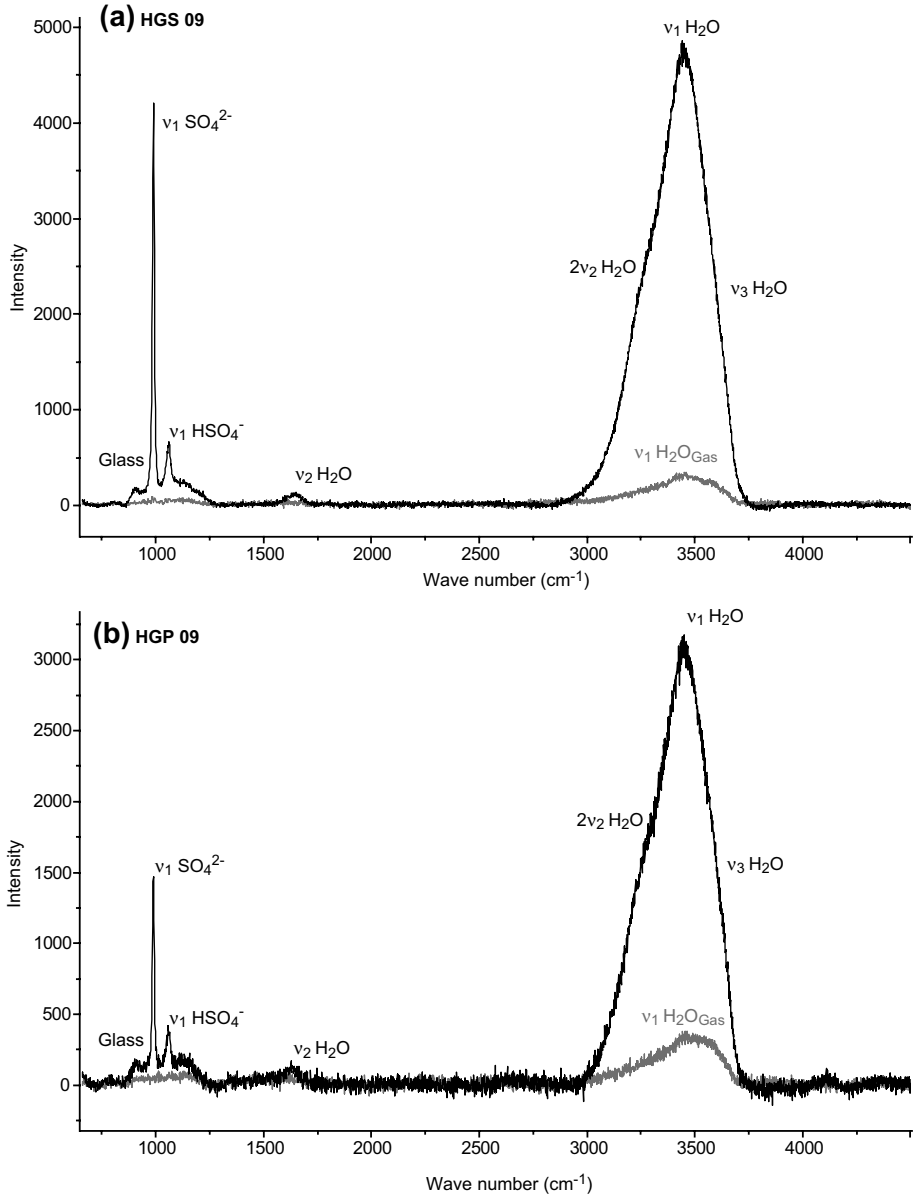

Fig. 13 Raman spectra of fluid inclusions from experiments in the system haplogranite–S–H_2O at Re–ReO_2 buffer conditions. Gray = gas phase; black = liquid phase. **a** Experiment HGS 09 with a peralkaline melt; **b** experiment HGP 09 with a peraluminous melt

implications for estimating the sulfur yield of explosive eruptions by satellite or ground-based remote-sensing techniques. Such methods usually only detect SO_2 (e.g. Francis et al. 1998; Oppenheimer et al. 2011; Theys et al. 2013) while the data from this study suggest that already at Re–ReO_2 buffer conditions, most of the sulfur is in the S^{6+} state. While some details of sulfur speciation—such as hydration numbers—may certainly change during quenching to room temperature, a change of oxidation state is unlikely to occur, since sulfur is the only element in the system that may have different oxidation states over the range of oxygen fugacity studied and, therefore, a redox exchange reaction with some other element during quenching is impossible. Moreover, the amounts of molecular O_2 or H_2 present in the fluid under run conditions are negligibly small compared to the sulfur concentrations, which excludes the possibility of a redox change by reaction with these species (see Binder and Keppler 2011 for a detailed discussion). The high oxidation state of sulfur as preserved in the fluid inclusions is, therefore, likely representative for the fluid at the *P, T* conditions inside a magma chamber. Interestingly, the sulfur in the quenched fluids from these experiments seems to be even more oxidized than in the study of Binder and Keppler (2011), which was conducted in a pure fluid system without coexisting silicate melt. According to the latter study, the change from a SO_2-dominated fluid to one that contains mostly S^{6+} occurs about one log unit in oxygen fugacity above the Re–ReO_2 buffer, while in the present experiments, only S^{6+} was detected already at this buffer. Possibly, the presence of alkali ions in the fluid stabilizes S^{6+} at lower

Table 2 Summary of the experimental results on the fluid/melt partitioning of sulfur at 750–850 °C and 200 MPa

System	Ni–NiO buffer	Re–ReO_2 buffer
Haplogranite–S–H_2O–CO_2 Al/(Na + K) = 0.93	$D_S^{fluid/melt}$ = 323 ± 14 No influence of CO_2	$D_S^{fluid/melt}$ = 74 ± 05 No influence of CO_2
Haplogranite–S–H_2O–NaCl Al/(Na + K) = 0.93	$D_S^{fluid/melt}$ = 264 ± 25 (x_{NaCl} = 0.1) $D_S^{fluid/melt}$ = 135 ± 14 (x_{NaCl} = 0.2) $D_S^{fluid/melt}$ = 84 ± 12 (x_{NaCl} = 0.3) $D_S^{fluid/melt}$ decreases with increasing NaCl	$D_S^{fluid/melt}$ = 128 ± 06 (x_{NaCl} = 0.1) $D_S^{fluid/melt}$ = 128 ± 06 (x_{NaCl} = 0.2) $D_S^{fluid/melt}$ = 128 ± 06 (x_{NaCl} = 0.3) No influence of NaCl Note: Compared to the NaCl-free system, the Al/(Na + K) ratio of the melt had increased, which explains the difference in $D_S^{fluid/melt}$
Haplogranite–S–H_2O		
Al/(Na + K) = 1.18	$D_S^{fluid/melt}$ = 508 ± 15	$D_S^{fluid/melt}$ = 246 ± 09
Al/(Na + K) = 0.93	$D_S^{fluid/melt}$ = 323 ± 14	$D_S^{fluid/melt}$ = 74 ± 05
Al/(Na + K) = 0.79	$D_S^{fluid/melt}$ = 257 ± 17	$D_S^{fluid/melt}$ = 96 ± 12
	$D_S^{fluid/melt}$ increases towards peraluminous compositions	$D_S^{fluid/melt}$ increases towards peraluminous compositions Note: The peralkaline melts preferentially lost Na_2O to the fluid, such that Al/(Na + K) approached 1

oxygen fugacities. This is plausible, since SO_3 is much more acidic than SO_2 and, therefore, the addition of a strongly alkaline component such as Na_2O to the system should shift the equilibrium towards SO_3 and its derivatives, such as H_2SO_4, HSO_4^-, and $NaSO_4^-$. If the oxidation state of sulfur does not change during an explosive eruption, the presence of abundant S^{6+} implies that the sulfur yield of some subduction zone volcanoes may be severely underestimated with conventional remote-sensing techniques. Indeed, the emission of near-source sulfate aerosols that may be direct condensation products of S^{6+}-bearing magmatic fluids has been reported for some smaller eruptions (e.g. Mather et al. 2004).

Acknowledgements This research was supported by DFG (Leibniz award to Hans Keppler). Constructive comments by an anonymous referee helped to improve the manuscript.

References

Beermann O, Botcharnikov RE, Nowak M (2015) Partitioning of sulfur and chlorine between aqueous fluid and basaltic melt at 1050 °C, 100 and 200 MPa. Chem Geol 418:132–157

Binder B, Keppler H (2011) The oxidation state of sulfur in magmatic fluids. Earth Planet Sci Lett 301:190–198

Black BA, Lamarque JF, Shields CA, Elkins-Tanton LT, Kiehl JT (2014) Acid rain and ozone depletion from pulsed Siberian Traps magmatism. Geology 42:67–70

Briffa KR, Jones PD, Schweingruber FH, Osborn TJ (1998) Influence of volcanic eruptions on Northern Hemisphere summer temperature over the past 600 years. Nature 393:450–455

Carroll MR, Rutherford MJ (1988) Sulfur speciation in hydrous experimental glasses of varying oxidation-state—results from measured wavelength shifts of sulfur X-rays. Am Mineral 73:845–849

Chou IM (1986) Permeability of precious metals to hydrogen at 2 kbar total pressure and elevated temperatures. Am J Sci 286:638–658

Devine JD, Sigurdsson H, Davis AN, Self S (1984) Estimates of sulfur and chlorine yield to the atmosphere from volcanic eruptions and potential climatic effects. J Geophys Res 89:6309–6325

Fiege A, Behrens H, Holtz F, Adams F (2014) Kinetic vs. thermodynamic control of degassing of H_2O–S +/- Cl-bearing andesitic melts. Geochim Cosmochim Acta 125:241–264

Fiege A, Holtz F, Behrens H, Mandeville CW, Shimizu N, Crede LS, Göttlicher J (2015) Experimental investigation of the S and S-isotope distribution between H_2O–S +/- Cl fluids and basaltic melts during decompression. Chem Geol 393–394:36–54

Francis P, Burton MR, Oppenheimer C (1998) Remote measurements of volcanic gas compositions by solar occultation spectroscopy. Nature 396:567–570

Gutiérrez X, Schiavi F, Keppler H (2016) The adsorption of HCl on volcanic ash. Earth Planet Sci Lett 438:66–74

Jugo PJ, Wilke M, Botcharnikov RE (2010) Sulfur K-edge XANES analysis of natural and synthetic basaltic glasses: implications for S speciation and S content as function of oxygen fugacity. Geochim Cosmochim Acta 74:5926–5938

Keppler H (1999) Experimental evidence for the source of excess sulfur in explosive volcanic eruptions. Science 284:1652–1654

Keppler H (2010) The distribution of sulfur between haplogranitic melts and aqueous fluids. Geochim Cosmochim Acta 74:645–660

Kerrick DM, Jacobs GK (1981) A modified Redlich–Kwong equation for H_2O, CO_2, and H_2O–CO_2 mixtures at elevated pressures and temperatures. Am J Sci 281:735–767

Lesne P, Kohn SC, Blundy J, Witham F, Botcharnikov RE, Behrens H (2011) Experimental simulation of closed system degassing in the system basalt–H_2O–CO_2–S–Cl. J Petrol 52:1737–1762

Masotta M, Keppler H (2015) Anhydrite solubility in differentiated arc magmas. Geochim Cosmochim Acta 158:79–102

Masotta M, Keppler H, Chaudhari A (2016) Fluid-melt partitioning of sulfur in differentiated arc magmas and the sulfur yield of explosive volcanic eruptions. Geochim Cosmochim Acta 176:26–43

Mather TA, Tsanev VI, Pyle DM, McGonigle AJS, Oppenheimer C, Allen AG (2004) Characterization and evolution of tropospheric plumes from Lascar and Villarrica volcanoes, Chile. J Geophys Res 109:D21303. https://doi.org/10.1029/2004JD004934

McCormick MP, Thomason LW, Trepte CR (1995) Atmospheric effects of the Mt Pinatubo eruption. Nature 373:399–404

McKenzie NR, Horton BK, Loomis SE, Stockli DF, Planavsky NJ, Lee CTA (2016) Continental arc volcanism as the principal driver of icehouse-greenhouse variability. Science 352:444–447

Ni H, Keppler H (2012) In-situ Raman spectroscopic study of sulfur speciation in oxidized magmatic-hydrothermal fluids. Am Mineral 97:1348–1353

Oppenheimer C, Scaillet B, Martin RS (2011) Sulfur degassing from volcanoes: source conditions, surveillance, plume chemistry and earth system impacts. Rev Mineral Geochem 73:363–421

Peltzer ET, Zhang X, Walz PM, Luna M, Brewer PG (2016) In situ Raman measurement of HS^- and H_2S in sediment porewaters and use of the HS^-:H_2S ratio as an indicator of pore water pH. Mar Chem 184:32–42

Robock A (2002) The climatic aftermath. Science 295:1242–1244

Sigl M, Winstrup M, McConnell JR, Welten KC, Plunkett G, Ludlow F, Buntgen U, Caffee M, Chellman N, Dahl-Jensen D, Fischer H, Kipfstuhl S, Kostick C, Maselli OJ, Mekhaldi F, Mulvaney R, Muscheler R, Pasteris DR, Pilcher JR, Salzer M, Schupbach S, Steffensen JP, Vinther BM, Woodruff TE (2015) Timing and climate forcing of volcanic eruptions for the past 2,500 years. Nature 523:543–549

Symonds RB, Rose WI, Bluth GJS, Gerlach TM (1994) Volcanic gas studies: methods, results, and applications. Rev Mineral 30:1–66

Theys N, Campion R, Clarisse L, Brenot H, van Gent J, Dils B, Corradini S, Merucci L, Coheur PF, van Roozendael M, Hurtmans D, Clerbaux C, S. Tait S, Ferrucci F (2013) Volcanic SO_2 fluxes derived from satellite data: a survey using OMI, GOME-2, IASI and MODIS. Atmos Chem Phys 13:5945–5968

Webster JD, Botcharnikov RE (2011) Distribution of sulfur between melt and fluid in S–O–H–C–Cl-bearing magmatic system at shallow crustal pressures and temperatures. Rev Mineral Geol 263:19–36

Webster JD, Sintini MF, de Vivo B (2009) The partitioning behavior of Cl, S, and H_2O in aqueous vapor- ± saline-liquid saturated phonolitic and trachytic melts at 200 MPa. Chem Geol 263:19–36

Webster JD, Goldoff B, Shimizu N (2011) C–O–H–S fluids and granitic magma: how S partitions and modifies CO_2 concentrations of fluid-saturated felsic melt at 200 MPa. Contrib Mineral Petrol 162:849–865

Wilke M, Klimm K, Kohn SC (2011) Spectroscopic studies on sulfur speciation in synthetic and natural glasses. Rev Mineral Geochem 73:41–78

Zajacz Z (2015) The effect of melt composition on the partitioning of oxidized sulfur between silicate melts and magmatic volatiles. Geochim Cosmochim Acta 158:223–244

Zajacz Z, Halter W (2009) Copper transport by high temperature, sulfur-rich magmatic vapor: evidence from silicate melt and vapor inclusions in a basaltic andesite from the Villarrica volcano (Chile). Earth Planet Sci Lett 282:115–121

Zajacz Z, Candela PA, Piccoli PM, Sanchez-Valle C (2012) The partitioning of sulfur and chlorine between andesite melts and magmatic volatiles and the exchange coefficients of major cations. Geochim Cosmochim Acta 89:81–101